Eur. Phys. J. C (2014) 74:2716
DOI 10.1140/epjc/s10052-014-2716-7

THE EUROPEAN PHYSICAL JOURNAL C

Regular Article - Theoretical Physics

Threshold resummation for the production of a color sextet (antitriplet) scalar at the LHC

Yong Chuan Zhan[1], **Ze Long Liu**[1], **Shi Ang Li**[1], **Chong Sheng Li**[1,2,a], **Hai Tao Li**[1]

[1] Department of Physics and State Key Laboratory of Nuclear Physics and Technology, Peking University, Beijing 100871, China
[2] Center for High Energy Physics, Peking University, Beijing 100871, China

Received: 10 August 2013 / Accepted: 23 December 2013 / Published online: 12 February 2014

Abstract We investigate threshold resummation effects in the production of a color sextet (antitriplet) scalar at next-to-next-to-leading logarithmic (NNLL) order at the LHC in the frame of soft-collinear effective theory. We show the total cross section and the rapidity distribution with NLO+NNLL accuracy, and we compare them with the NLO results. Besides, we use recent dijet data at the LHC to give the constraints on the couplings between the colored scalars and quarks.

1 Introduction

There is no clear evidence of new physics beyond the Standard Model found at the LHC so far [1–3], and the most favored supersymmetry, extra dimensions, and many others all receive somewhat strong constraints [1,4,5]. Then it is a preferable way to be more concerned about the model independent theory rather than considering some specific models. Here we study the model independent color sextet (antitriplet) scalars, which have many significant effects in the phenomenology. Actually, color sextet scalars have been included in many new physics models, such as unification theories [6–8], supersymmetry with R-parity violation [9], and diquark Higgs [10]. Their masses can be as low as the TeV scale or less [11], which leads to much impact on the physics. For example, in the supersymmetric Pati–Salam $SU(2)_R \times SU(2)_L \times SU(4)_C$ model, light color sextet scalars can be realized around the weak scale even though the scale of $SU(2)_R \times SU(4)_C$; symmetry breaking is around 10^{10} GeV [10,11]. Observation of the color sextet scalars will be a direct signal of new physics beyond the Standard Model.

Considering the interaction of the color sextet (antitriplet) scalars with quarks, which is parameterized, the relevant Lagrangian can be written as [12]

$$\mathcal{L} = 2\sqrt{2}\left[\bar{K}_i^{ab}\phi^i\bar{\psi}_a.(\lambda_L P_L + \lambda_R P_R).\psi_b^C + h.c.\right] + \left(D_\mu^{ij}\phi_j\right)^\dagger D_\mu^{ik}\phi_k - m_\phi^2\phi^{i\dagger}\phi^i, \quad (1)$$

where K_i^{ab} is the Clebsch–Gordan coefficient of the sextet (antitriplet), $\lambda_{L/R}$ is the Yukawa-like coupling, and a, b are the color indices. The quantum numbers of the colored scalars are listed in Table 1, and more information can be found in [12,13].

In order to satisfy the gauge symmetry, the colored scalars couple to same-sign quarks, and then they have fractional electronic charges. In the cases of antitriplet the couplings should be antisymmetric in flavor. For convenience, we label the colored scalars as $sextet^{\mathrm{I}}$, $sextet^{\mathrm{II}}$ and $sextet^{\mathrm{III}}$ with electronic charge $1/3$, $-2/3$ and $4/3$, respectively. For the antitriplet, the labels are $antitriplet^{I}$, $antitriplet^{II}$ and $antitriplet^{III}$.

It has been shown [10,14,15] that the measurements of $D^0 - \bar{D}^0$ mixing and the rate of $D \to \pi^+\pi^0(\pi^+\phi)$ decay can constrain the couplings of the colored scalars to two up-type quarks: $\lambda_{\mathrm{R}}^{uu}, \lambda_{\mathrm{R}}^{uc} \lesssim 0.1$, $|\mathrm{Re}(\lambda^{cc}\lambda^{uu*})| \sim 5.76 \times 10^{-7}$ for $m_\phi \sim 1$ TeV. Besides, the left-handed coupling λ_{L} also receives a tight constraint due to minimal flavor violation. Since we use the model independent coupling $\lambda^2 = \lambda_{\mathrm{L}}^2 + \lambda_{\mathrm{R}}^2$, the above constraints can be relaxed in the scenario considered below.

Production and decay of the colored scalars at hadron colliders have been extensively discussed in [12,15–20]. Recently the CMS collaboration has searched for the signal of the colored scalar and obtained limits on the production cross section of such resonant states [21–23] with the fixed-order theoretical predictions (leading order and next-to-leading order) in Ref. [18,24]. In this paper we investigate the threshold resummation effects in the single production of the color sextet (antitriplet) scalars, and we also discuss the rapidity distribution of the colored scalars at NLO+NNLL accuracy at the LHC with soft-collinear effec-

[a] e-mail: csli@pku.edu.cn

Table 1 Q is the $SU(2)_L$ quark doublet, and U(D) is the up(down)-type $SU(2)_L$ quark singlet

$SU(2)_L$	$U(1)_Y$	$\|Q\| = \|T_3 + Y\|$	Couplings to
1	1/3	1/3	QQ,UD
3	1/3	1/3, 2/3, 4/3	QQ
1	−2/3	2/3	DD
1	4/3	4/3	UU

Under $SU(3)_C \times SU(2)_L \times U(1)_Y$, Q has the quantum numbers (**3**,**2**, 1/6), while U has (**3**,**1**,2/3), and D has (**3**,**1**,−1/3)

tive theory (SCET) [25–29]. As a cross check, we also calculate the NLO corrections using the analytical phase-space integral method, and we present their analytical expressions. Actually, when the masses of the colored scalars approach the threshold limit, there are large logarithms left after cancelling the divergences, because the scale of the soft gluon radiations is rather small compared to the scalar mass. These threshold logarithms should be resummed to reduce the scale uncertainties and improve the confidence of the theoretical predictions.

This paper is organized as follows: In Sect. 2, we present the NLO calculations. In Sect. 3, we briefly show the factorization in the threshold limit of the production of the colored scalar. In Sect. 4, we calculate the soft function and present solutions of the renormalization group equations obeyed by hard and soft functions. In Sect. 5, we present detailed numerical analyses and compare the NLO+NNLL rapidity distributions with the NLO results. We also use recent dijet data at the LHC to give constraints on the couplings between the colored scalars and quarks. We conclude in Sect. 6.

2 Fixed-order calculations

We consider the process $h_1 + h_2 \to \phi + X$, where h_1 and h_2 are the incoming hadrons with momenta P_1 and P_2, and we define the rapidity of the colored scalar ϕ as $Y = \frac{1}{2}\ln\frac{E+p_z}{E-p_z}$, where E and p_z represent the energy and longitudinal momentum of the scalar in the center-of-mass frame of the colliding hadrons. We write the cross section as [30,31]

$$\frac{\mathrm{d}\sigma}{\mathrm{d}Y} = \sum_{ij}\int_\tau^1 \frac{\mathrm{d}z}{z}\int_0^1 \mathrm{d}y\; f_{i/h_1}(x_1,\mu_f) f_{j/h_2}(x_2,\mu_f) C_{ij}(y,z,m_\phi,\mu_f), \tag{2}$$

$$\begin{aligned} C_{ij}(y,z,m_\phi,\mu_f) &= z\left|\frac{\mathrm{d}x_1\mathrm{d}x_2}{\mathrm{d}y\mathrm{d}z}\right|\frac{\mathrm{d}\sigma_{ij}}{\mathrm{d}Y} \\ &= \frac{1}{2S}\int \mathrm{d}PS_f\;\overline{|\mathcal{M}_{ij}|^2} \\ &\quad \delta\left(y - \frac{u'-z}{(1-z)(1+u')}\right), \end{aligned} \tag{3}$$

with

$$\begin{aligned} &S = (P_1+P_2)^2,\ \tau = m_\phi^2/S,\ s = (p_1+p_2)^2 = x_1x_2S, \\ &u' = \frac{x_1}{x_2}\mathrm{e}^{-2Y},\ z = \frac{m_\phi^2}{s} = \frac{\tau}{x_1x_2}, \\ &y = \frac{u'-z}{(1-z)(1+u')}, \end{aligned} \tag{4}$$

where PS_f is the final state phase space, and μ_f is the factorization scale. For a one-particle final state, there is no y dependence, and then the delta function can be reduced to $(\delta(y)+\delta(1-y))/2$.

The NLO corrections were investigated in Ref. [12] using the phase-space slicing method [32,33]. Here we recalculate the matrix elements, which are consistent with the results in Ref. [12], and we do not present the details of these calculations. Below we just show the analytical expressions of the phase-space integration. Using the identity

$$x^{-1+\epsilon} = \frac{1}{\epsilon}\delta(x) + \sum_n \frac{\epsilon^n}{n!}\left[\frac{\ln^n x}{x}\right]_+, \tag{5}$$

with

$$\begin{aligned} \int_\tau^1 \mathrm{d}x\left[\frac{\ln^n(1-x)}{1-x}\right]_+ f(x) &= \int_\tau^1 \mathrm{d}x\frac{\ln^n(1-x)}{1-x}[f(x)-f(1)] \\ &\quad - f(1)\int_0^\tau \mathrm{d}x\frac{\ln^n(1-x)}{1-x}, \end{aligned} \tag{6}$$

we can obtain the following results for $C_{ij}(y,z,m_\phi,\mu_f)$. The leading-order result is

$$C_{qq}^{(0)} = \frac{2\pi\lambda^2 N_D}{N_C^2 S}\frac{\delta(y)+\delta(1-y)}{2}\delta(1-z), \tag{7}$$

and the contributions from the virtual and real corrections for the qq channel are given by

$$\begin{aligned} C_{qq}^{\mathrm{virt}} &= \frac{2\pi\lambda^2 N_D}{N_C^2 S}\frac{\delta(y)+\delta(1-y)}{2}\delta(1-z)\frac{\alpha_s}{4\pi}\frac{(4\pi)^\epsilon}{\Gamma(1-\epsilon)} \\ &\quad \times\left[\frac{-4C_F}{\epsilon^2} + \frac{1}{\epsilon}(-2C_D - 6C_F + 4C_F L)\right. \\ &\quad \left. + C_D\left(2L - 2 - \frac{4\pi^2}{3}\right) + C_F\left(-2L^2 - 4 + 2\pi^2\right)\right] \end{aligned} \tag{8}$$

and

$$
\begin{aligned}
&C_{qq}^{\text{real}} \\
&= \frac{2\pi\lambda^2 N_D}{N_C^2 S}\frac{\alpha_s}{4\pi}\frac{(4\pi)^\epsilon}{\Gamma(1-\epsilon)}\left\{\frac{\delta(y)+\delta(1-y)}{2}\delta(1-z)\frac{4C_F}{\epsilon^2}\right. \\
&+\frac{\delta(y)+\delta(1-y)}{2}\frac{1}{\epsilon}\left((2C_D-4C_FL)\delta(1-z)\right. \\
&-8C_F\left[\frac{1}{1-z}\right]_+ +4C_F(1+z)\Big) \\
&+C_D\left[\frac{\delta(y)+\delta(1-y)}{2}\delta(1-z)(-2L+4)\right. \\
&-4\left[\frac{1}{1-z}\right]_+ +2z+2\Big]+C_F\frac{\delta(y)+\delta(1-y)}{2} \\
&\times\left[\delta(1-z)\left(2L^2-\frac{2\pi^2}{3}\right)+8\,(L-\ln(z))\left[\frac{1}{1-z}\right]_+\right. \\
&+16\left[\frac{\ln(1-z)}{1-z}\right]_+ -4(1+z)(L+2\ln(1-z) \\
&\left.-\ln(z))+4(1-z)\right]+C_F\left(\left[\frac{1}{y}\right]_+ +\left[\frac{1}{1-y}\right]_+\right) \\
&\left.\times\left(4\left[\frac{1}{1-z}\right]_+ -2(1+z)\right)\right\},
\end{aligned}
\tag{9}
$$

respectively. Combining the contributions of the LO results, the virtual and real corrections, we obtain the bare NLO partonic differential cross sections:

$$
C_{qq}^{\text{bare}} = C_{qq}^{(0)} + C_{qq}^{\text{virt}} + C_{qq}^{\text{real}}. \tag{10}
$$

They still contain the collinear singularities, which can be factorized into the following form to all orders of perturbation theory in general:

$$
\begin{aligned}
C_{ij}^{\text{bare}}(z,1/\epsilon) &= \sum_{k,l}\Gamma_{ki}(z,\mu_f,1/\epsilon) \\
&\otimes\Gamma_{lj}(z,\mu_f,1/\epsilon)\otimes C_{kl}(z,\mu_f),
\end{aligned}
\tag{11}
$$

where μ_f is the factorization scale and $\otimes$ is the convolution symbol defined as

$$
f(z)\otimes g(z) = \int_z^1 \frac{\mathrm{d}y}{y} f(y) g\left(\frac{z}{y}\right). \tag{12}
$$

The universal splitting functions $\Gamma_{ij}(z,\mu_f,1/\epsilon)$ represent the probability of finding a particle i with fraction z of the longitudinal momentum inside the parent particle j at the scale μ_f. They contain the collinear divergences, and they can be absorbed into the redefinition of the PDF according to mass factorization [34,35]. Adopting the $\overline{MS}$ mass-factorization scheme, we have to $\mathcal{O}(\alpha_s)$

$$
\begin{aligned}
\Gamma_{ij}(z,\mu_f,1/\epsilon) &= \delta_{ij}\delta(1-z) - \frac{1}{\epsilon}\frac{\alpha_s}{2\pi}\frac{\Gamma(1-\epsilon)}{\Gamma(1-2\epsilon)} \\
&\times\left(\frac{4\pi\mu_r^2}{\mu_f^2}\right)^\epsilon P_{ij}^{(0)}(z),
\end{aligned}
\tag{13}
$$

where $P_{ij}^{(0)}(z)$ are the leading-order Altarelli–Parisi splitting functions [36]

$$
\begin{aligned}
P_{qq}^{(0)}(z) &= \frac{4}{3}\left[\frac{1+z^2}{(1-z)_+}+\frac{3}{2}\delta(1-z)\right], \\
P_{qg}^{(0)}(z) &= \frac{1}{2}[(1-z)^2+z^2].
\end{aligned}
\tag{14}
$$

After absorbing the splitting functions $\Gamma_{ij}(z,\mu_f,1/\epsilon)$ into the redefinition of the PDFs through the mass factorization in this way, we have the hard-scattering partonic differential cross sections $C_{ij}(y,z,m_\phi,\mu_f)$, which are free of collinear divergences and depend on the scale μ_f. The final NLO results for the qq channel are given by

$$
\begin{aligned}
C_{qq}^{(1)} &= \frac{2\pi\lambda^2 N_D}{N_C^2 S}\frac{\alpha s}{4\pi}\left\{\frac{\delta(y)+\delta(1-y)}{2}\right. \\
&\times\left[\delta(1-z)\left(C_D\left(2-\frac{4}{3}\pi^2\right)+C_F\left(\frac{4}{3}\pi^2-4\right)\right)\right. \\
&-8C_F(\ln z-L)\left[\frac{1}{1-z}\right]_+ +16C_F\left[\frac{\ln(1-z)}{1-z}\right]_+ \\
&-4C_F\left((z+1)L+2(z+1)\ln(1-z)\right. \\
&\left.-(z+1)\ln z+z-1)\right]-2C_F\left[\frac{1}{y}\right]_+ \\
&\times\left(-2\left[\frac{1}{1-z}\right]_+ +z+1\right) \\
&-2C_F\left[\frac{1}{1-y}\right]_+\left(-2\left[\frac{1}{1-z}\right]_+ +z+1\right) \\
&\left.+2C_D\left(-2\left[\frac{1}{1-z}\right]_+ +z+1\right)\right\}.
\end{aligned}
\tag{15}
$$

Similarly, the final NLO result for the qg channel is given by

$$
\begin{aligned}
C_{qg}^{(1)} &= \frac{2\pi\lambda^2 N_D}{N_C(N_C^2-1)S}\frac{\alpha_s}{4\pi}\left\{\delta(1-y)2C_F\left[(2z^2-2z+1)\right.\right. \\
&\times(L+2\ln(1-z)-\ln z-1)+1] \\
&+2C_F\left[\frac{1}{1-y}\right]_+(2z^2-2z+1) \\
&+\frac{2(1-z)}{(yz-y-z)^2}\left[C_D\left(y^2(z-1)^2+z^2\right)\right. \\
&\left.\left.+C_F(y+1)(z-1)(yz-y-z)^2\right]\right\},
\end{aligned}
\tag{16}
$$

where $\lambda^2=\lambda_L^2+\lambda_R^2$, $L=\ln(m_\phi^2/\mu_f^2)$. The color factors are $N_D=6$, $C_D=10/3$ for the sextet and $N_D=3$, $C_D=4/3$ for the antitriplet. In the above results, we have set the renormalization scale $\mu_r=\mu_f$. Finally, we combine these

finite results to arrive at the NLO differential cross section $C_{ij}(y, z, m_\phi, \mu_f)$ for colored scalar production:

$$C_{ij} = C_{qq}^{(0)} + C_{qq}^{(1)} + C_{qg}^{(1)}. \tag{17}$$

Following the method in [30], we rearrange the results as

$$\begin{aligned} C_{qq}(z, y, m_\phi, \mu_f) &= C_{qq}^{(0)} + C_{qq}^{(1)} \\ &= \frac{2\pi N_D}{S N_C^2} \frac{\delta(y) + \delta(1-y)}{2} C(z, m_\phi, \mu_f) + C_{qq}^{\text{subleading}}, \end{aligned} \tag{18}$$

where the $C(z, m_\phi, \mu_f)$ are the leading singular terms (threshold terms), which are arranged as

$$\begin{aligned} &C(z, m_\phi, \mu_f) \\ &= \lambda^2 \delta[1-z] + \lambda^2 \frac{\alpha_s}{4\pi} \left\{ \delta[1-z] \left[C_D \left(2 - \frac{4}{3}\pi^2 \right) \right. \right. \\ &\quad \left. + C_F \left(-4 + \frac{4}{3}\pi^2 \right) \right] \\ &\quad + \left[\frac{1}{1-z} \right]_+ [-4 C_D + 8 C_F (L - \ln z)] \\ &\quad \left. + \left[\frac{\ln(1-z)}{1-z} \right]_+ 16 C_F \right\}. \end{aligned} \tag{19}$$

From Eq. (19), we can see that the singular terms make the perturbative series badly convergent in the threshold limit $z \to 1$, and thus they must be resummed to all orders.

3 Factorization at threshold in SCET

The production of the colored scalar involves several scales, which are

$$s, m_\phi^2 \gg s(1-z)^2 \gg \Lambda_{QCD}^2 \tag{20}$$

in the threshold limit, and it is convenient to introduce two light-like vectors n and $\bar{n}$ along the directions of the colliding partons, which satisfy $n \cdot \bar{n} = 2$. In the lab frame, they can be written as

$$n = (1, 0, 0, 1), \quad \bar{n} = (1, 0, 0, -1). \tag{21}$$

Then any four vector can be decomposed as

$$k^\mu = n \cdot k \frac{\bar{n}^\mu}{2} + \bar{n} \cdot k \frac{n^\mu}{2} + k_\perp^\mu \equiv k^+ \frac{\bar{n}^\mu}{2} + k^- \frac{n^\mu}{2} + k_\perp^\mu. \tag{22}$$

In this limit, we need to distinguish four different momentum regions:

$$\begin{aligned} &\text{hard: } k^\mu \sim \sqrt{s}(1, 1, 1), \\ &\text{hard-collinear: } k^\mu \sim \sqrt{s}(\epsilon, 1, \sqrt{\epsilon}), \\ &\text{anti-hard-collinear: } k^\mu \sim \sqrt{s}(1, \epsilon, \sqrt{\epsilon}), \\ &\text{soft: } k^\mu \sim \sqrt{s}(\epsilon, \epsilon, \epsilon), \end{aligned} \tag{23}$$

where we use $k^\mu = (k^+, k^-, k_\perp)$ to denote the momenta and $\epsilon = (1-z) \ll 1$.

Generally, the differential cross section can be written as

$$\begin{aligned} \mathrm{d}\sigma = &\frac{1}{2S} \frac{\mathrm{d}^3 \mathbf{q}}{(2\pi)^3 2E_\phi} \int \mathrm{d}^4 x \langle N_1(P_1) N_2(P_2) | \mathcal{H}_{\text{eff}}^\dagger(x) | \phi(q) \rangle \\ &\times \langle \phi(q) | \mathcal{H}_{\text{eff}}(0) | N_1(P_1) N_2(P_2) \rangle, \end{aligned} \tag{24}$$

where the effective Hamiltonian is given by

$$\mathcal{H}_{\text{eff}}(x) = \int \mathrm{d}t_1 \mathrm{d}t_2 \, \mathrm{e}^{i m_\phi v \cdot x} \, \tilde{C}(t_1, t_2) \, \mathcal{O}(x, t_1, t_2), \tag{25}$$

with

$$\begin{aligned} \mathcal{O}(x, t_1, t_2) = &2\sqrt{2} \, Y_{\bar{n}}^{a\dagger} \bar{\chi}_{\bar{n}}(x + t_2 n) \cdot (\lambda_{\mathrm{L}} P_{\mathrm{L}} + \lambda_{\mathrm{R}} P_{\mathrm{R}}) \cdot \\ &\times Y_n^{b\dagger} \chi_n^C (x + t_1 \bar{n}) \, Y_v^i \phi_v(x) \, K_i^{ab}, \end{aligned} \tag{26}$$

where χ_n is the gauge-invariant combination of the n-collinear quark field and n-collinear Wilson line, and Y is defined as the soft Wilson line [26,37,38]:

$$\begin{aligned} Y_n(x) &= \mathcal{P} \exp \left(i g_s \int_{-\infty}^{0} \mathrm{d}t_0 \, n \cdot A_s^a(x + t_0 n) t^a \right), \\ Y_v(x) &= \mathcal{P} \exp \left(-i g_s \int_{0}^{\infty} \mathrm{d}t_0 \, v \cdot A_s^a(x + t_0 v) t^a \right), \end{aligned} \tag{27}$$

where v is the velocity of the colored scalar. The matrix element can be factorized as follows:

$$\begin{aligned} &\langle N_1(P_1) N_2(P_2) | \mathcal{O}^\dagger(x) \mathcal{O}(0) | N_1(P_1) N_2(P_2) \rangle \\ &= \frac{2\lambda^2 N_D}{N_C^2} \left\langle N_1(P_1) | \bar{\chi}_n(x) \frac{\bar{n}\!\!\!/}{2} \chi_n(0) | N_1(P_1) \right\rangle \\ &\quad \times \left\langle N_2(P_2) | \bar{\chi}_{\bar{n}}(x) \frac{n\!\!\!/}{2} \chi_{\bar{n}}(0) | N_2(P_2) \right\rangle \hat{\mathcal{W}}(x, \mu_f), \end{aligned} \tag{28}$$

with

$$\begin{aligned} \hat{\mathcal{W}}(x, \mu_f) = &\frac{1}{N_D} \left\langle 0 \left| \mathrm{Tr} \left\{ \bar{T} \left[Y_n^\dagger(x) Y_{\bar{n}}^\dagger(x) Y_v(x) \right] \right. \right. \right. \\ &\left. \left. \left. \times T \left[Y_{\bar{n}}(0) Y_n(0) Y_v^\dagger(0) \right] \right\} \right| 0 \right\rangle, \end{aligned} \tag{29}$$

where the trace is over color indices, and $\bar{T}$ denotes the anti-time-ordering operator. The initial state collinear sector reduces to the conventional PDFs [26,39]:

$$f_{i/N}(x, \mu) = \frac{1}{2\pi} \int \mathrm{d}t \, \mathrm{e}^{-i x t \bar{n} \cdot p} \left\langle N(p) \left| \bar{\chi}(t\bar{n}) \frac{\bar{n}\!\!\!/}{2} \chi(0) \right| N(p) \right\rangle. \tag{30}$$

The integrals over t_1 and t_2 produce the Fourier-transformed Wilson coefficients:

$$C_H(-\bar{n} \cdot p_1 \, n \cdot p_2, \mu_f) = \int \mathrm{d}t_1 \mathrm{d}t_2 \mathrm{e}^{-i t_1 \bar{n} \cdot p_1 - i t_2 n \cdot p_2} \tilde{C}(t_1, t_2, \mu_f). \tag{31}$$

Finally, the singular differential cross section in the threshold region can be written as

$$\frac{\mathrm{d}\sigma}{\mathrm{d}Y} = \frac{2\pi N_D}{SN_C^2} \sum_{i,j} \int_\tau^1 \frac{\mathrm{d}z}{z} \int_0^1 \mathrm{d}y \; f_{i/h_1}(x_1,\mu_f) f_{j/h_2}(x_2,\mu_f) \times \frac{\delta(y)+\delta(1-y)}{2} C(z,m_\phi,\mu_f).$$

Following the approach in Ref. [40], $C(z,m_\phi,\mu_f)$ can be factorized as

$$C(z,m_\phi,\mu_f) = \lambda^2(\mu_f)\mathbf{H}(m_\phi,\mu_f)\mathbf{S}\left(\sqrt{s}(1-z),\mu_f\right), \tag{32}$$

with

$$\begin{aligned}
&\mathbf{H}(m_\phi,\mu_f) = \left|C_H(-m_\phi^2 - i\epsilon,\mu_f)\right|^2,\\
&\mathbf{S}\left(\sqrt{s}(1-z),\mu_f\right) = \sqrt{s}\,\mathcal{W}\left(\sqrt{s}(1-z),\mu_f\right),\\
&\mathcal{W}(\omega,\mu_f) = \int \frac{\mathrm{d}x^0}{4\pi}\, \mathrm{e}^{i\omega x^0/2}\, \hat{\mathcal{W}}(x^0,\mathbf{x}=0,\mu_f).
\end{aligned} \tag{33}$$

The soft and collinear degrees of freedom decouple in the threshold limit, so the physics at different scales can be studied separately [26].

4 Resummation

The coupling λ satisfies the renormalization group equation

$$\frac{\mathrm{d}}{\mathrm{d}\ln\mu}\lambda(\mu) = \gamma^\lambda(\alpha_s)\lambda(\mu), \tag{34}$$

where the one-loop level γ^λ is

$$\gamma^\lambda = -\frac{\alpha_s}{4\pi}6C_F. \tag{35}$$

The hard function encodes short distance information,

$$\begin{aligned}
\mathbf{H}(m_\phi,\mu_f) &= \left|C_H(-m_\phi^2 - i\epsilon,\mu_f)\right|^2\\
&= 1 + \sum_{n=1}^{\infty} c_n(L)\left(\frac{\alpha_s(\mu_f)}{4\pi}\right)^n.
\end{aligned} \tag{36}$$

We read off the results from the virtual correction:

$$\mathbf{H}(m_\phi,\mu_f) = 1 + \frac{\alpha_s}{4\pi}\left[C_D\left(2L - \frac{4}{3}\pi^2 - 2\right) + C_F\left(-2L^2 + \frac{7}{3}\pi^2 - 4\right)\right]. \tag{37}$$

C_H satisfies the RGE [30]

$$\frac{\mathrm{d}}{\mathrm{d}\ln\mu}C_H(-m^2 - i\epsilon,\mu) = \left[\Gamma_{\mathrm{cusp}}(\alpha_s)\left(\ln\frac{m^2}{\mu^2} - i\pi\right) + \gamma^H(\alpha_s)\right]C_H(-m^2 - i\epsilon,\mu), \tag{38}$$

with

$$\gamma^H = 2\gamma^q + \gamma^D - \gamma^\lambda. \tag{39}$$

γ^q is the anomalous dimension of the massless quark [41], and γ^D is the one of the final state colored scalar, which is given by [42]

$$\begin{aligned}
&\gamma_0^D = -2C_D,\\
&\gamma_1^D = C_D C_A\left(\frac{2\pi^2}{3} - \frac{98}{9} - 4\zeta_3\right) + \frac{40}{9}C_D T_F n_f.
\end{aligned} \tag{40}$$

The solution of Eq. (38) is [30]

$$C_H(-m_\phi^2,\mu_f) = \exp\left[2S(\mu_h,\mu_f) - a_{\gamma^H}(\mu_h,\mu_f) + i\pi a_\Gamma(\mu_h,\mu_f)\right]\left(\frac{m_\phi^2}{\mu_h^2}\right)^{-a_\Gamma(\mu_h,\mu_f)} C_H(-m_\phi^2,\mu_h), \tag{41}$$

with

$$S(\nu,\mu) = -\int_{\alpha_s(\nu)}^{\alpha_s(\mu)} \mathrm{d}\alpha \frac{\Gamma_{\mathrm{cusp}}(\alpha)}{\beta(\alpha)} \int_{\alpha_s(\nu)}^{\alpha} \frac{\mathrm{d}\alpha'}{\beta(\alpha')}, \tag{42}$$

$$a_\Gamma(\nu,\mu) = -\int_{\alpha_s(\nu)}^{\alpha_s(\mu)} \mathrm{d}\alpha \frac{\Gamma_{\mathrm{cusp}}(\alpha)}{\beta(\alpha)}, \tag{43}$$

where μ_h is the hard matching scale, and for a_{γ^H} we have a similar expression.

Up to the NLO, the soft matrix elements accounting for soft gluon radiations from initial and final states can be obtained after calculating the Feynman diagrams shown in Fig. 1, and the soft function is given by

$$\begin{aligned}
&\mathbf{S}(\sqrt{s}(1-z),\mu_f)\\
&= \frac{\alpha_s}{4\pi}\left[\delta(1-z)\left(C_D(-2L+4) + C_F(2L^2 - \pi^2)\right) + (-4C_D + 8C_F(L - \ln z))\left[\frac{1}{1-z}\right]_+ + 16C_F\left[\frac{\ln(1-z)}{1-z}\right]_+\right].
\end{aligned} \tag{44}$$

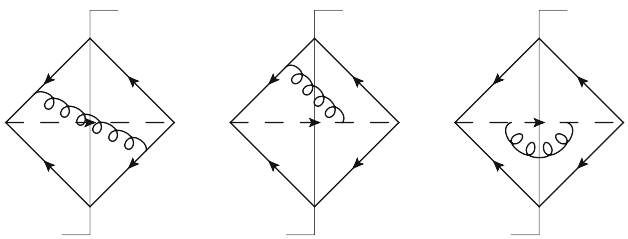

Fig. 1 Diagrams for calculating the $\mathcal{O}(\alpha_s)$ soft function. The *solid lines* represent Wilson lines in the light-like n and $\bar{n}$ directions, the *dashed lines* represent Wilson lines in the v direction, and the *cut curly lines* represent the cut gluon propagators

Table 2 Schemes for resummation with different levels of accuracy

RG-impr.PT	Log.approx	Accuracy $\sim \alpha_s^n L^k$	Γ_{cusp}	$\gamma^H, \gamma^\phi, \gamma^\lambda$	$C_H, \tilde{s}$
–	LL	$k = 2n$	1-loop	Tree-level	Tree-level
LO	NLL	$2n - 1 \leq k \leq 2n$	2-loop	1-loop	Tree-level
NLO	NNLL	$2n - 3 \leq k \leq 2n$	3-loop	2-loop	1-loop

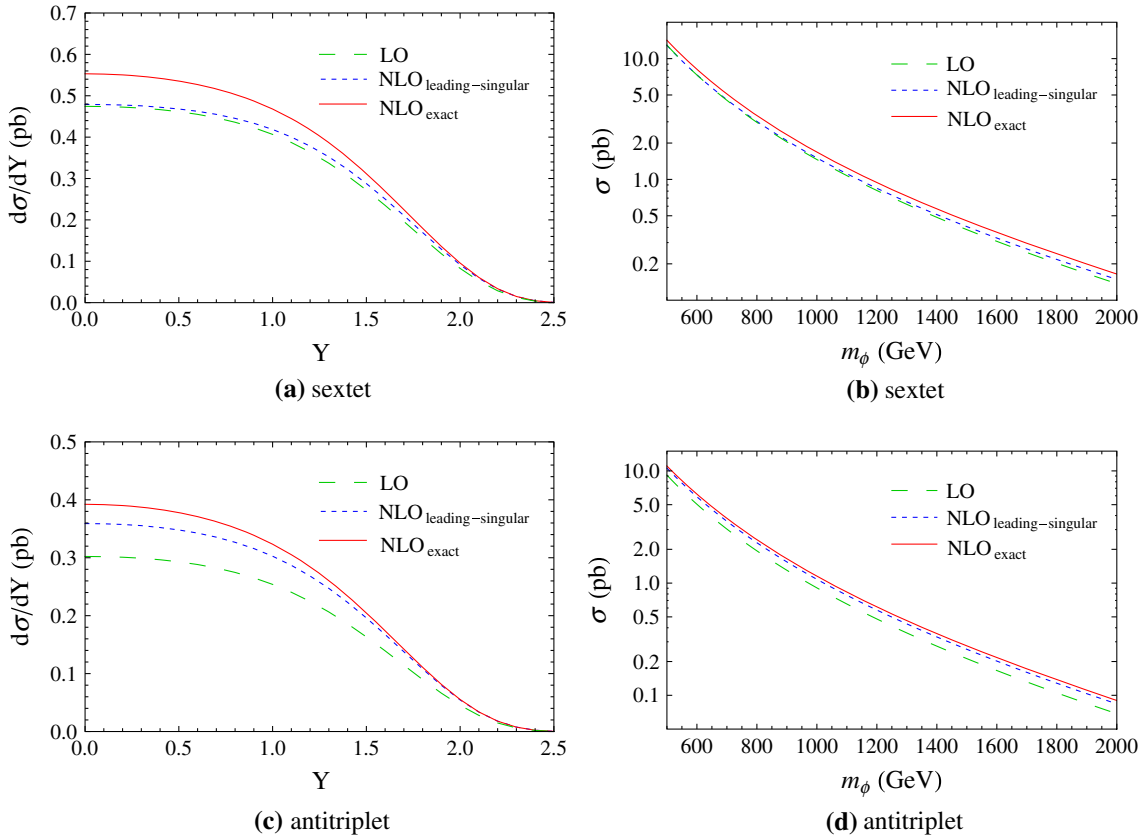

(a) sextet **(b)** sextet **(c)** antitriplet **(d)** antitriplet

Fig. 2 Comparison of the exact NLO results and the leading singular results. The *long-dashed*, *dashed* and *solid lines* correspond to LO, leading singular NLO and exact NLO results, respectively. The mass of the colored scalars is set to be 1 TeV in the rapidity distributions, and the center-of-mass energy of the colliding hadrons is set to be 14 TeV

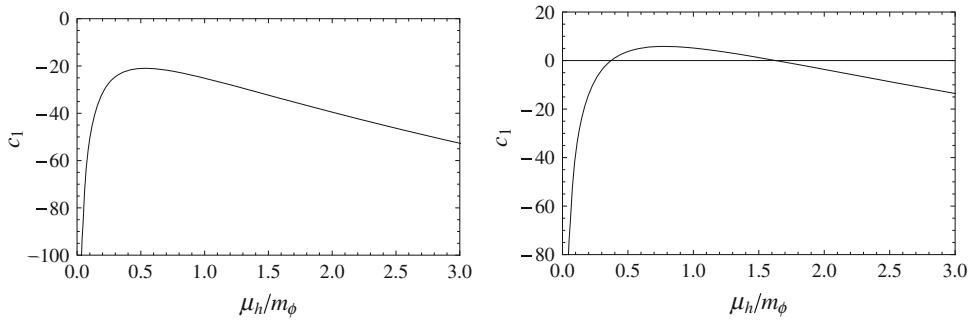

(a) sextet **(b)** antitriplet

Fig. 3 The μ_h dependence of the expansion coefficients c_1 in the hard function

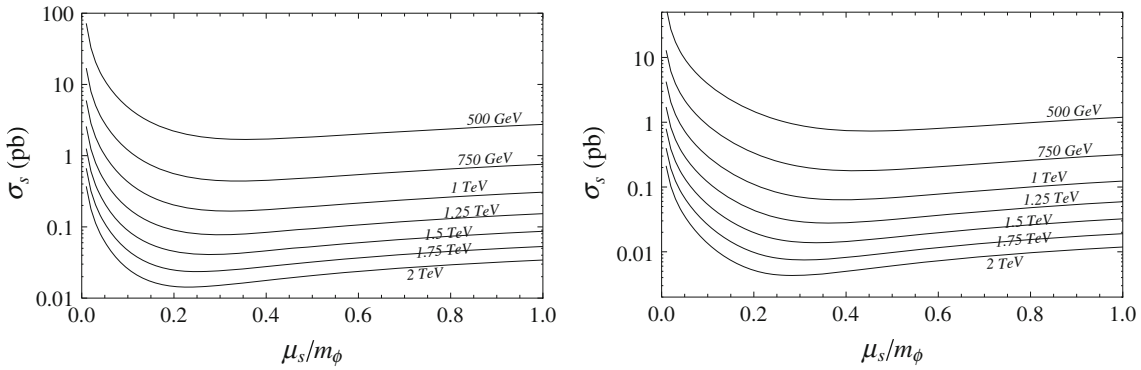

(a) sextet **(b)** antitriplet

Fig. 4 The μ_s dependence of the soft function with different masses of the colored scalars

Table 3 Numerical results of the total cross section (unit: pb)

m_ϕ (TeV)	$\sqrt{S}$ = 8 TeV			$\sqrt{S}$ = 14 TeV		
	LO	NLO	NLO+NNLL$_{\text{approx}}$	LO	NLO	NLO+NNLL$_{\text{approx}}$
Sextet						
0.5	7.53	8.59	8.58	12.9	14.2	14.2
1	0.768	0.916	0.918	1.46	1.68	1.68
2	0.0416	0.0512	0.0529	0.137	0.165	0.165
Antitriplet						
0.5	4.85	6.13	6.21	9.17	11.1	11.2
1	0.406	0.532	0.542	0.907	1.15	1.17
2	0.0161	0.0215	0.0225	0.0686	0.899	0.916

It satisfies the RGE [30]

$$\frac{\mathrm{d}\,\mathcal{W}(\omega,\mu)}{\mathrm{d}\ln\mu} = -\left[4\Gamma_{\text{cusp}}(\alpha_s)\ln\frac{\omega}{\mu} + 2\gamma^W(\alpha_s)\right]\mathcal{W}(\omega,\mu) - 4\Gamma_{\text{cusp}}(\alpha_s)\int_0^\omega \mathrm{d}\omega'\frac{\mathcal{W}(\omega',\mu)-\mathcal{W}(\omega,\mu)}{\omega-\omega'}, \tag{45}$$

with

$$\gamma^W = 2\gamma^\phi + \gamma^H + \gamma^\lambda, \tag{46}$$

where γ^ϕ is the anomalous dimension of the PDF [43]. Its solution is [30]

$$\mathcal{W}(\omega,\mu_f) = \exp\left[-4S(\mu_s,\mu_f) + 2a_{\gamma^W}(\mu_s,\mu_f)\right] \times \tilde{s}(\partial_\eta,\mu_s)\frac{1}{\omega}\left(\frac{\omega}{\mu_s}\right)^{2\eta}\frac{\mathrm{e}^{-2\gamma_E\eta}}{\Gamma(2\eta)}, \tag{47}$$

with

$$\eta = 2a_\Gamma(\mu_s,\mu_f), \tag{48}$$

where ∂_η is the derivative with respect to η, and $\tilde{s}$ is obtained by a Laplace transformation:

$$\tilde{s}(L,\mu_s) = \int_0^\infty \mathrm{d}\omega\mathrm{e}^{-s\omega}\mathcal{W}(\omega,\mu_s) = 1 + \frac{\alpha_s}{4\pi}\left[C_D(-2L+4) + C_F\left(2L^2+\frac{4}{3}\pi^2\right)\right], \tag{49}$$

with

$$s = \frac{1}{\mathrm{e}^{\gamma_E}\mu_s\mathrm{e}^{L/2}}. \tag{50}$$

Combining the above formulas, the RG-improved integral kernel is given by

$$C(z,m_\phi,\mu_f) = \lambda^2(\mu_\lambda)|C_H(-m_\phi^2,\mu_h)|^2U(m_\phi,\mu_\lambda,\mu_h,\mu_s,\mu_f) \cdot\frac{z^{-\eta}}{(1-z)^{1-2\eta}}\tilde{s}\left(\ln\frac{m_\phi^2(1-z)^2}{\mu_s^2 z}+\partial_\eta\,,\ \mu_s\right)\frac{\mathrm{e}^{-2\gamma_E\eta}}{\Gamma(2\eta)}, \tag{51}$$

with

$$U(m,\mu_\lambda,\mu_h,\mu_s,\mu_f) = \left(\frac{m^2}{\mu_h^2}\right)^{-2a_\Gamma(\mu_h,\mu_s)} \exp\left[4S(\mu_h,\mu_s)+4a_{\gamma^\phi}(\mu_s,\mu_f) - 2a_{\gamma^H}(\mu_h,\mu_s)-2a_{\gamma^\lambda}(\mu_\lambda,\mu_s)\right]. \quad (52)$$

For convenience, we list the counting scheme in Table 2, which shows corresponding requirements of different levels of accuracy [30]. Currently the two-loop γ^λ is not available in the literature, so we just use the one-loop γ^λ. The contribution of γ^λ in the evolution function $U(m,\mu_\lambda,\mu_h,\mu_s,\mu_f)$ cancels out when $\mu_\lambda \sim \mu_h$, so γ^λ only affects the running of $\lambda(\mu_\lambda)$, which gives a subordinate contribution. We then call our resummation an approximate next-to-next-to-leading logarithmic (NNLL$_{\rm approx}$), which is combined with the NLO results as follows:

$$\frac{d\sigma^{\rm combined}}{dY} = \frac{d\sigma^{\rm thresh}}{dY}\bigg|_{\mu_\lambda,\mu_h,\mu_s,\mu_f} + \left(\frac{d\sigma^{\rm fixed\text{-}order}}{dY}\bigg|_{\mu_f} - \frac{d\sigma^{\rm thresh}}{dY}\bigg|_{\mu_\lambda=\mu_h=\mu_s=\mu_f}\right). \quad (53)$$

5 Numerical discussion

In this section, we discuss the numerical results for threshold resummation effects in the single production of the color sextet (antitriplet) scalars at the LHC. Throughout our work the PDF sets MSTW2008lo and MSTW2008nlo [44–46] are used for LO, NLL and NLO, and NNLL$_{\rm approx}$, respectively. If not explained specially, we will assume the coupling $\lambda^2(M_Z) = 0.01\alpha_s(M_Z)$, and we choose the initial state quarks uu for the sextet and ud for the antitriplet.

The comparison between the leading singular results and the NLO results is shown in Fig. 2. We find that the leading singular terms give the dominant contribution, and the leading singular contribution of the sextet is smaller than the one of the antitriplet. The reason is that the terms associated with C_D give a negative contribution, and then a larger C_D of the sextet leads to smaller leading singular results.

Taking the perturbative convergence of C_H and $\tilde{s}$ as the guiding principle, we can obtain the matching scales μ_h and μ_s. In Fig. 3 we show the μ_h dependence of the expansion coefficient c_1 defined in Eq. (36). We choose the hard scale $\mu_h^0 = 0.535 m_\phi$ for the sextet and $\mu_h^0 = 1.63 m_\phi$ for the antitriplet, respectively.

The μ_s dependence of the soft function is shown in Fig. 4. We fit the results and obtain the empirical functions:

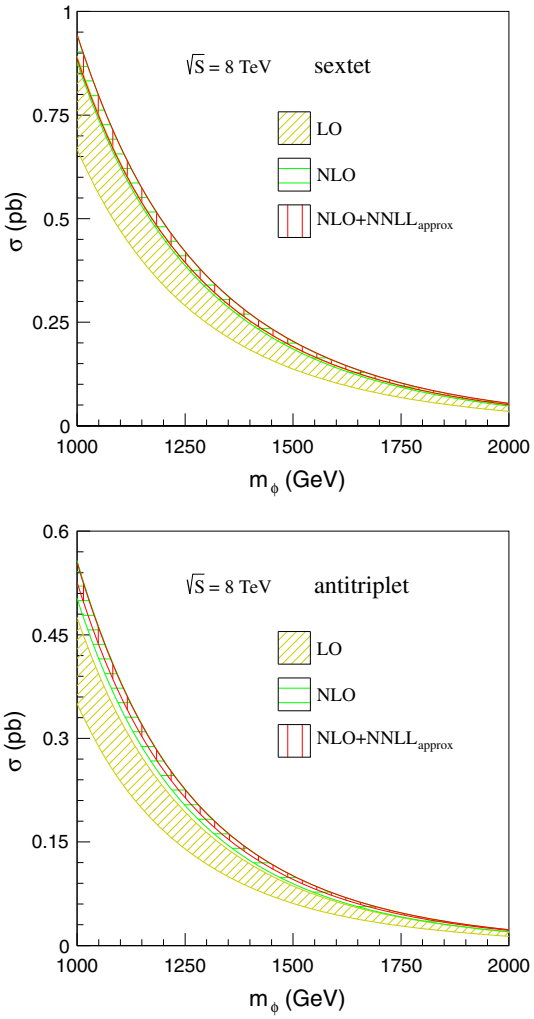

Fig. 5 The fixed-order and RG-improved cross section predictions including perturbative uncertainty bands due to variations of scale μ_f

$$\text{sextet: } \mu_s^0 = \frac{m_\phi(1-\tau)}{\sqrt{7+540\tau}}, \qquad \text{antitriplet: } \mu_s^0 = \frac{m_\phi(1-\tau)}{\sqrt{4.6+362\tau}}. \quad (54)$$

It is required that μ_λ reflects the intensity of the interaction between the colored scalars and quarks, and $\mu_\lambda = \mu_h$ is reasonable.

In Table 3, we list the typical results of the total cross sections, which compare NLO+NNLL$_{\rm approx}$ with LO and NLO results. From Table 3, we can see that the resummation effects increase the NLO total cross section by about 2 and 0.2 % for the 1 TeV antitriplet and sextet, respectively, and 5 and 3 % for the 2 TeV antitriplet and sextet, respectively, at the 8 TeV LHC. The resummation effects at the 14 TeV LHC are smaller than the ones at the 8 TeV LHC.

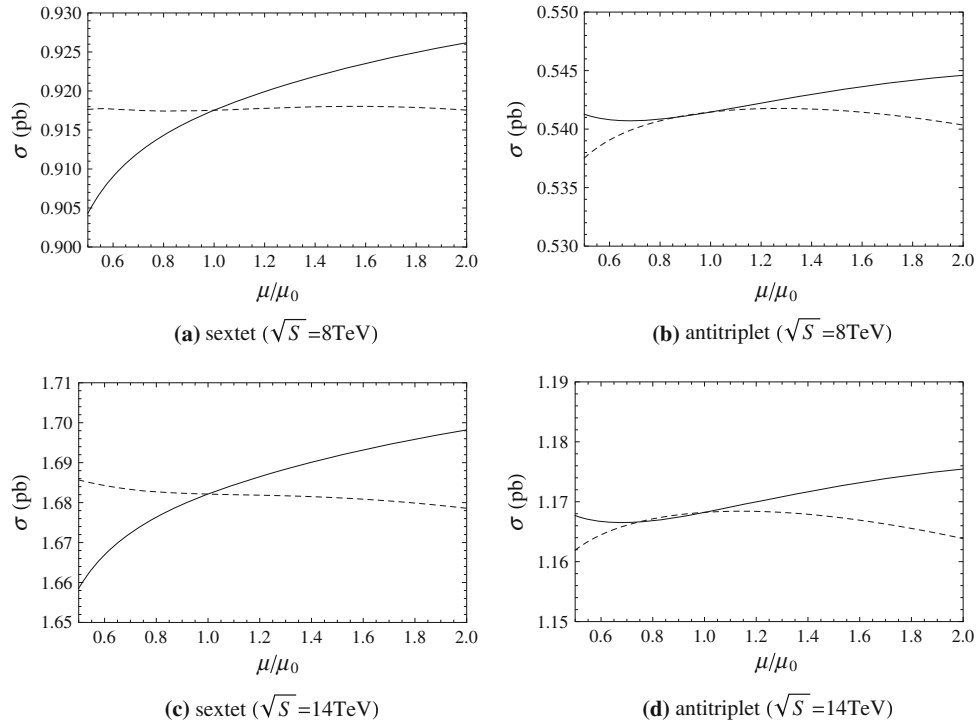

Fig. 6 The μ_h and μ_s dependence of the resummed total cross sections. The *solid* and *dashed lines* represent the μ_h and μ_s dependence, respectively. We set the scalar mass to 1 TeV

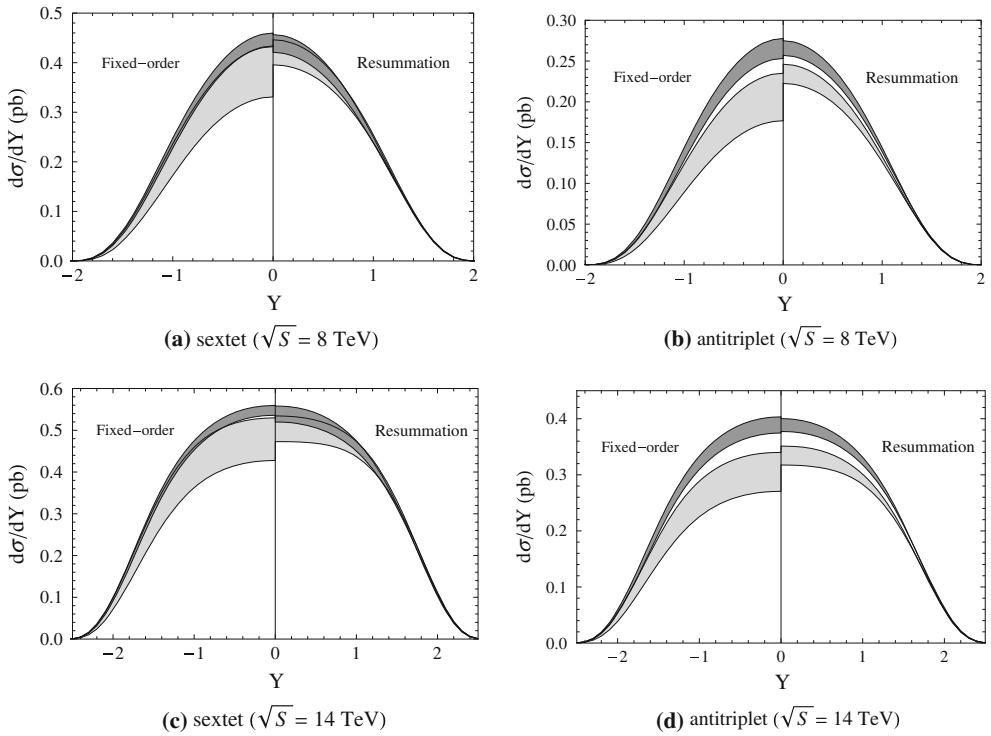

Fig. 7 The comparison of the rapidity distributions is between the combined resummation results and the fixed-order results for the sextet and the antitriplet. The scalar mass is set to 1 TeV. The lighter bands stand for LO and NLL, while the darker bands represent NLO and $\text{NNLL}_{\text{approx}}$

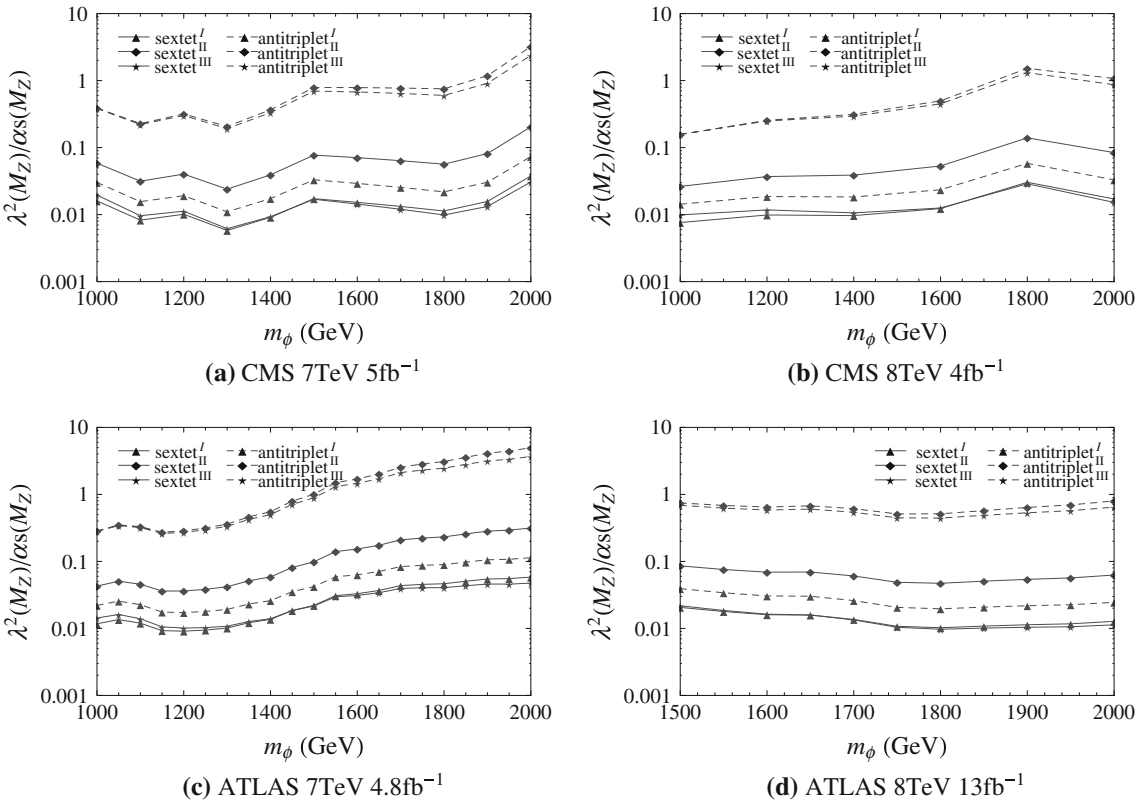

(a) CMS 7TeV 5fb^{-1} **(b)** CMS 8TeV 4fb^{-1}

(c) ATLAS 7TeV 4.8fb^{-1} **(d)** ATLAS 8TeV 13fb^{-1}

Fig. 8 Constraint on the couplings λ of the colored scalars with different electronic charges

In Fig. 5, we show the dependence of the total cross section on the scalar masses including perturbative uncertainty bands due to variation of scale μ_f at the 8 TeV LHC. We find that the threshold resummation reduces the scale dependence of the total cross section. The scenario at the 14 TeV LHC is very similar, so we do not present it in the figures.

Figure 6 shows the dependence of the resummed total cross section on μ_h and μ_s. The scales are varied over the ranges $\mu_h^0/2 < \mu_h < 2\mu_h^0$ and $\mu_s^0/2 < \mu_s < 2\mu_s^0$, respectively. From Fig. 6, we can see that the μ_h dependence of the sextet is more sensitive than the antitriplet.

In Fig. 7, we present the rapidity distributions, which compare the resummation results combined in Eq. (53) with the fixed-order results. The scale μ_f is varied over the range $m_\phi/2 < \mu_f < 2m_\phi$. We find that the shapes of the rapidity distribution of the resummation change slightly over the fixed-order results, and resummation reduces the scale dependence, except the NNLL$_{\text{approx}}$ results of the sextet cases. This is caused by the large color factor for the sextet ($C_D = 10/3$ for the sextet, $C_D = 4/3$ for the antitriplet). The terms containing a large color factor C_D, which is associated with the scale dependence of λ and α_s, will enlarge the scale dependence of the NNLL$_{\text{approx}}$ results of the sextet.

Finally, we use recent dijet data at the LHC to give constraints on the couplings λ. The CMS collaboration published the results of dijet production based on 5 fb^{-1} of 7 TeV data and 4 fb^{-1} of 8 TeV data [21–23], and the ATLAS collaboration based on 4.8 fb^{-1} of 7 TeV data and 13 fb^{-1} of 8 TeV data [47,48]. Using the narrow-width-approximation [49], the total cross section can be written as

$$\begin{aligned}\sigma &= \frac{(2\pi)^7}{2S}\int_{q^2_{min}}^{q^2_{max}} \mathrm{d}q^2 \int \mathrm{d}\phi_p\, \mathrm{d}\phi_d \left|\mathcal{M}_p(q^2)\right|^2 \\ &\quad\times \left[(q^2-m^2)^2+(m\Gamma)^2\right]^{-1} \left|\mathcal{M}_d(q^2)\right|^2 \\ &= \frac{(2\pi)^8}{4Sm\Gamma}\int \mathrm{d}\phi_p \left|\mathcal{M}_p(q^2)\right|^2 \int \mathrm{d}\phi_d \left|\mathcal{M}_d(q^2)\right|^2.\end{aligned} \tag{55}$$

After fitting the dijet data, we can give the constraints on the couplings. Since there is no direct theoretical requirement on the couplings between the colored scalars and different quarks, we use a common value for the coupling λ here. The colored scalars with different electronic charges couple to different quarks, and then they receive different constraints. In Fig. 8, we show the results of the constraints on the couplings. The most stringent constraint on $sextet^I$ is $\lambda^2(M_Z) \geq 0.006\alpha_s(M_Z)$, and similarly the other constraints are $0.024\alpha_s(M_Z)$, $0.006\alpha_s(M_Z)$, $0.011\alpha_s(M_Z)$, $0.16\alpha_s(M_Z)$, and $0.16\alpha_s(M_Z)$ for $sextet^{II}$,

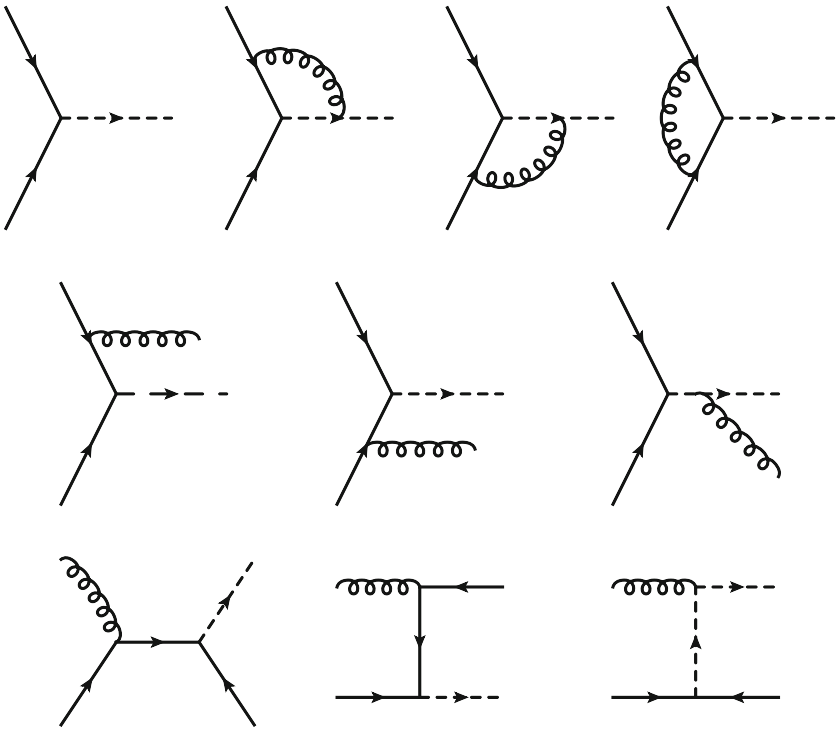

Fig. 9 Relevant Feynman diagrams for the production of the colored scalar

$sextet^{III}$, $antitriplet^{I}$, $antitriplet^{II}$, and $antitriplet^{III}$, respectively.

6 Conclusion

We have studied the threshold resummation effects in the single production of the color sextet (antitriplet) scalars at the LHC with the soft-collinear effective theory. We find that the resummation effects increase the NLO total cross section by about 2 and 0.2 % for 1 TeV color antitriplet and sextet scalar, respectively, and 5 and 3 % for 2 TeV color antitriplet and sextet scalar, respectively, at the 8 TeV LHC. The resummation effects improve the scale dependence of the cross section and the rapidity distribution generally. But in the case of the rapidity distribution of the color sextet scalar, the scale dependence is not improved because of the large color factor C_D ($C_D = 10/3$ for the sextet, $C_D = 4/3$ for the antitriplet) enlarging the scale dependence. Besides, we use recent dijet data from the LHC to give constraints on the couplings. For different colored scalars with different electronic charges, the most stringent constraints of $\lambda^2(M_Z)$ range from $0.006\alpha_s(M_Z)$ to $0.16\ \alpha_s(M_Z)$.

Acknowledgments We would like to thank Hua Xing Zhu, Jian Wang, and Qing Hong Cao for useful discussions. This work was supported in part by the National Natural Science Foundation of China, under Grants No. 11021092 and No. 11135003.

Appendix : Relevant Feynman Diagrams

Relevant Feynman diagrams for the production of the colored scalar are shown in Fig. 9.

References

1. A. Mete, ATL-PHYS-PROC-2012-201, ATL-COM-PHYS-2012-1365 (2012).
2. O. Vickey Boeriu, ATL-PHYS-PROC-2012-051, ATL-COM-PHYS-2012-313 (2012)
3. T. Lari, ATL-PHYS-PROC-2011-150, ATL-COM-PHYS-2011-1340 (2011)
4. ATLAS. https://twiki.cern.ch/twiki/bin/view/AtlasPublic/CombinedSummaryPlots (2012)
5. CMS. https://twiki.cern.ch/twiki/bin/view/CMSPublic/PhysicsResults (2012)
6. J.C. Pati, A. Salam, Phys. Rev. D **10**, 275 (1974)
7. R.N. Mohapatra, R. Marshak, Phys. Rev. Lett. **44**, 1316 (1980)
8. P. Fileviez, Perez. Phys. Lett. B **654**, 189 (2007). [arXiv:hep-ph/0702287]
9. R. Barbier, C. Berat, M. Besancon, M. Chemtob, A. Deandrea et al., Phys. Rep. 4 **20**, 1 (2005). [arXiv:hep-ph/0406039]
10. R. Mohapatra, N. Okada, H.-B. Yu, Phys. Rev. D **77**, 011701 (2008). [arXiv:0709.1486]
11. Z. Chacko, R. Mohapatra, Phys. Rev. D **59**, 055004 (1999). [arXiv:hep-ph/9802388]

12. T. Han, I. Lewis, T. McElmurry, JHEP **123**, 1001 (2010) [arXiv:0909.2666]
13. E. Del Nobile, R. Franceschini, D. Pappadopulo, A. Strumia, Nucl. Phys. B **826**, 217 (2010) [arXiv:0908.1567]
14. C.-H. Chen, Phys. Lett. B **680**, 133 (2009). [arXiv:0902.2620]
15. C.-R. Chen, W. Klemm, V. Rentala, K. Wang, Phys. Rev. D **79**, 054002 (2009). [arXiv:0811.2105]
16. I. Gogoladze, Y. Mimura, N. Okada, Q. Shafi, Phys. Lett. B **686**, 233 (2010). [arXiv:1001.5260]
17. E.L. Berger, Q.-H. Cao, C.-R. Chen, G. Shaughnessy, H. Zhang, Phys. Rev. Lett. **105**, 181802 (2010). [arXiv:1005.2622]
18. T. Han, I. Lewis, Z. Liu, JHEP **085**, 1012 (2010) [arXiv:1010.4309]
19. P. Richardson, D. Winn, Eur. Phys. J. C **72**, 2012 (1862). [arXiv:1108.6154]
20. D. Karabacak, S. Nandi, S.K. Rai, Phys. Rev. D **85**, 075011 (2012). [arXiv:1201.2917]
21. S. Chatrchyan et al. (CMS Collaboration), JHEP **1301**, 013 (2013) [arXiv:1210.2387]
22. S. Chatrchyan et al. (CMS Collaboration) (2013) [arXiv:1302.4794]
23. Tech. Rep. CMS-PAS-EXO-12-059, CERN, Geneva (2013)
24. J.L. Hewett, T.G. Rizzo, Phys. Rep. **183**, 193 (1989)
25. C.W. Bauer, S. Fleming, D. Pirjol, I.W. Stewart, Phys. Rev. D **63**, 114020 (2001). [arXiv:hep-ph/0011336]
26. C.W. Bauer, D. Pirjol, I.W. Stewart, Phys. Rev. D **65**, 054022 (2002). [arXiv:hep-ph/0109045]
27. M. Beneke, A. Chapovsky, M. Diehl, T. Feldmann, Nucl. Phys. B **643**, 431 (2002). [arXiv:hep-ph/0206152]
28. C.W. Bauer, S. Fleming, M.E. Luke, Phys. Rev. D **63**, 014006 (2000). [arXiv:hep-ph/0005275]
29. C.W. Bauer, S. Fleming, D. Pirjol, I.Z. Rothstein, I.W. Stewart, Phys. Rev. D **66**, 014017 (2002). [arXiv:hep-ph/0202088]
30. T. Becher, M. Neubert, G. Xu, JHEP **0807**, 030 (2008) [arXiv:0710.0680]
31. C. Anastasiou, L.J. Dixon, K. Melnikov, F. Petriello, Phys. Rev. D **69**, 094008 (2004). [arXiv:hep-ph/0312266]
32. H. Baer, J. Ohnemus, J. Owens, Phys. Lett. B **234**, 127 (1990)
33. B. Harris, J. Owens, Phys. Rev. D **65**, 094032 (2002). [arXiv:hep-ph/0102128]
34. J.C. Collins, D.E. Soper, G.F. Sterman, Nucl. Phys. B **261**, 104 (1985)
35. G.T. Bodwin, Phys. Rev. D **31**, 2616 (1985)
36. G. Altarelli, G. Parisi, Nucl. Phys. B **126**, 298 (1977)
37. R.J. Hill, M. Neubert, Nucl. Phys. B **657**, 229 (2003). [arXiv:hep-ph/0211018]
38. T. Becher, R.J. Hill, M. Neubert, Phys. Rev. D **69**, 054017 (2004). [arXiv:hep-ph/0308122]
39. J.C. Collins, D.E. Soper, Nucl. Phys. B **194**, 445 (1982)
40. V. Ahrens, T. Becher, M. Neubert, L.L. Yang, Eur. Phys. J C **62**, 333 (2009). [arXiv:0809.4283]
41. T. Gehrmann, T. Huber, D. Maitre, Phys. Lett. B **622**, 295 (2005). [arXiv:hep-ph/0507061]
42. T. Becher, M. Neubert, Phys. Rev. D **79**, 125004 (2009). [arXiv:0904.1021]
43. S. Moch, J. Vermaseren, A. Vogt, Nucl. Phys. B **688**, 101 (2004). [arXiv:hep-ph/0403192]
44. A. Martin, W. Stirling, R. Thorne, G. Watt, Eur. Phys. J. C **63**, 189 (2009). [arXiv:0901.0002]
45. A. Martin, W. Stirling, R. Thorne, G. Watt, Eur. Phys. J. C **64**, 653 (2009). [arXiv:0905.3531]
46. A. Martin, W. Stirling, R. Thorne, G. Watt, Eur. Phys. J. C **70**, 51 (2010). [arXiv:1007.2624]
47. G. Aad et al. (ATLAS Collaboration), JHEP **1301**, 029 (2013) [arXiv:1210.1718]
48. Tech. Rep. ATLAS-CONF-2012-148, CERN, Geneva (2012).
49. N. Kauer, Phys. Lett. **B649**, 413 (2007). [arXiv:hep-ph/0703077]